

NUMERICAL EVALUATION OF THE INFLUENCE OF UPSTREAM BENDS CURVATURE ON ULTRASONIC FLOW METER k-FACTOR

Ramon Silva Martins, ramonsmartins@gmail.com

Rogério Ramos, ramosrogerio@hotmail.com

LFTC, PPGEM, Department of Mechanical Engineering, Universidade Federal do Espírito Santo.

Av. Fernando Ferrari, 405. Vitória – ES CEP 29075-910

Telephone number: +55 27 40092641 / Fax: +55 27 40092650

Abstract. Oil and gas industry needs accurate measurement since such flows are regulated by law. In these industries some pipe installation effects, generated by its configuration, are usual to be faced. Hence flow disturbances occur and measurement accuracy is committed. The paper presents a preliminary evaluation of ultrasonic flow meter k-factor for single bend and double bend out-of-plane pipe configuration, which have been tested for different curvature radii (0.5D, 1.0D, 1.5D and 2.0D) upstream of the metering section. Reynolds numbers varies from 8,000 to 200,000. A numerical approach has been used in order to estimate k-factors via computational fluid dynamics (CFD). The k- ϵ turbulence model has been used. Previous results are graphically shown and commented. The k-factors simulated have not shown any direct clear influence of curvature radius.

Keywords: k-factor, installation effects, bend curvature radius, ultrasonic flow meter, numerical simulation

1. INTRODUCTION

Flow meters calibration is an important issue in oil and gas industry, where accurate flow measurements are required and regulations describe the proceedings for operational and custody metering. These documents, such as AGA Report N° 9 (1998) and the Brazilian federal regulation Portaria Conjunta ANP/INMETRO N° 1 (2000), point the ultrasonic flow meter (UFM) as a suitable technology for gas metering. In offshore oil rigs, UFM's are commonly used to flare gas flow control. Still, the conditions for accurate flow measurements may be not reliable due to several obstacles, such as bends, valves and diameter changes. In many cases, such obstacles are close to the metering section, due to available space, causing flow disturbances. Since the majority of flow meters suppose by their measurement principle fully developed flow condition, the metering is thus compromised.

Scientific community has been evaluating flow disturbances patterns and consequences as well as methods to diminish flow measurement errors and uncertainties. Ruppel and Peters (2004) and Mickan *et al.* (1997) identify downstream flow patterns of typical pipe installation by means of experiments. Hilgenstock and Ernst (1996) compare computational fluid dynamics (CFD) results and experiments, pointing numerical simulations as interesting tools for meters calibration and diagnostic. Holm *et al.* (1995) proposed the calculation of a numerical k-factor in order to evaluate various installation effects on UFM's.

Although the single bend and the double bend out-of-plane are the most classic pipe configuration for installation effects, the influence of the curvature radius of these bends on flow measurements is still subject of technical research. According to its measurement principle, UFM is relatively sensitive to flow profile disturbances. Two ultrasonic transducers compose a single channel with a certain inclination (α) to the pipe axis transmit and receive ultrasonic pulses through the fluid (Fig. 1).

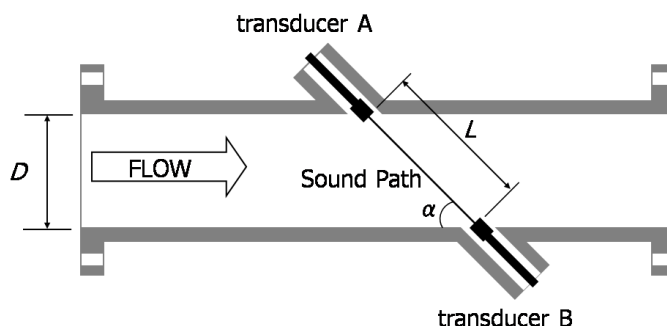


Figure 1. Ultrasonic flow meter scheme.

Supposing a non-flow situation, transit time – time to the ultrasonic pulse travel from a transducer to the other – and distance between the transducers (L) may give the sound propagation velocity in the fluid (c). Once there is a flow velocity field, transit times become different due to the signal deviation. That makes downstream pulse transit time, which goes from transducer A to B (t_{AB}), shorter than upstream pulse, which goes from transducer B to A (t_{BA}), since the

last one propagates against the flow. Since transducers distance (L), diameter (D) and transit times (t_{AB} and t_{BA}), are known variables, calculation of transit mean velocities (v_{AB} and v_{BA}) are possible and they are given by Eqs. (1) and (2).

$$v_{AB} = \frac{L}{t_{AB}} = c + V_{SP} \cos \alpha \quad (1)$$

$$v_{BA} = \frac{L}{t_{BA}} = c - V_{SP} \cos \alpha \quad (2)$$

V_{SP} is the flow mean velocity in sound path direction. The unknowns V_{SP} and c can be found by solving the algebraic system of Eqs. (1) and (2) and the result is shown in Eqs. (3) and (4).

$$c = \frac{D}{2 \sin \alpha} \left(\frac{t_{AB} + t_{BA}}{t_{AB} t_{BA}} \right) \quad (3)$$

$$V_{SP} = \frac{D}{\sin 2\alpha} \left(\frac{t_{AB} - t_{BA}}{t_{AB} t_{BA}} \right) \quad (4)$$

Due to their measurement principle, ultrasonic flow meters calculate c and V_{SP} , nevertheless the flow mean velocity (V_m) is useful on flow rate calculation. V_m depends on flow profile and a correction factor (k) is used to obtain it from V_{SP} as shown in Eq. (5). (AGA Report N° 9, 1998)

$$V_m = k V_{SP} \quad (5)$$

The aim of the paper is to analyze the behavior of a numerical k-factor – as proposed by Holm *et al.* (1995) – for several curvature radii of single bend (SB) and double bend (DB) out-of-plane pipe configurations. Reynolds number has also been changed in order to check for flow and disturbances patterns.

2. MATHEMATICAL MODEL AND NUMERICAL SIMULATION PARAMETERS

This section presents the governing equations used in mathematical model, the boundary conditions, the geometry configurations and mesh, and the numerical method used to solve.

2.1. Conservation equations

Considering stationary flow, fluid incompressibility and constant viscosity conditions, the turbulent flow may be predicted by the mass conservation equation and the momentum conservation equation. These equations are presented in indicial notation by Eqs. (6) and (7), respectively.

$$\frac{\partial(\rho V_i)}{\partial x_i} = 0 \quad (6)$$

$$\rho \frac{\partial(\bar{V}_i \bar{V}_j)}{\partial x_i} = \frac{\partial p}{\partial x_j} + \frac{\partial}{\partial x_i} \left[(\mu + \mu_T) \left(\frac{\partial \bar{V}_i}{\partial x_j} + \frac{\partial \bar{V}_j}{\partial x_i} \right) \right] \quad (7)$$

Where ρ is the fluid density, V_i is the velocity component in direction i , \bar{V}_i is the turbulent mean velocity in direction i , μ is the dynamic viscosity and μ_T is the turbulent viscosity, given by the turbulence model.

2.2. Turbulence modeling

The momentum equation considering turbulence needs additional equations to be solved. These equations come from the turbulence model. In this paper the k - ϵ model has been applied. This model uses the Boussinesq hypothesis, which considerate the turbulent viscosity (μ_T) for the relation between the Reynolds stresses tensor and the turbulent mean velocity, as shown in Eq. (8).

$$\tau_{Tij} = \mu_T \left(\frac{\partial \bar{V}_i}{\partial x_j} + \frac{\partial \bar{V}_j}{\partial x_i} \right) \quad (8)$$

Where τ_{Tij} is the Reynolds stresses tensor. Two transport equations must be solved in order to obtain μ_T : Eq. (9) for k (turbulence kinetic energy) and Eq. (10) for ε (turbulence eddy dissipation).

$$\rho \frac{\partial(\bar{V}_i k)}{\partial x_j} = \frac{\partial}{\partial x_j} \left[\left(\mu + \frac{\mu_T}{\sigma_k} \right) \frac{\partial k}{\partial x_i} \right] + P_k - \rho \varepsilon \quad (9)$$

$$\rho \frac{\partial(\bar{V}_i \varepsilon)}{\partial x_j} = \frac{\partial}{\partial x_j} \left[\left(\mu + \frac{\mu_T}{\sigma_\varepsilon} \right) \frac{\partial \varepsilon}{\partial x_i} \right] + \frac{\varepsilon}{k} (C_{\varepsilon 1} P_k - C_{\varepsilon 2} \rho \varepsilon) \quad (10)$$

Where P_k is obtained from Eq. (11), σ_k , σ_ε , $C_{\varepsilon 1}$ and $C_{\varepsilon 2}$ are constants of the model and their values are presented in Tab. 1.

$$P_k = \mu_T \frac{\partial \bar{V}_i}{\partial x_j} \left(\frac{\partial \bar{V}_i}{\partial x_j} + \frac{\partial \bar{V}_j}{\partial x_i} \right) \quad (11)$$

The turbulent viscosity (μ_T) is finally obtained from Eq. (12).

$$\mu_T = C_\mu \rho \frac{k^2}{\varepsilon} \quad (12)$$

Where C_μ is also a constant of the model and its value is presented in Tab. 1, as well. (ANSYS CFXTM Version 11.0, 2007)

Table 1. Constants for the k - ε model.

σ_k	σ_ε	$C_{\varepsilon 1}$	$C_{\varepsilon 2}$	C_μ
1.0	1.3	1.44	1.92	0.09

2.3. Geometries and meshes

Pipe configurations and parameters proposed in this paper are the same used by Holm *et al.* (1995), except for the curvature radii. In all cases internal diameter of 20.4 mm and transducers inclination (α) of 45 ° have been used. Figures 2 and 3, respectively, show the single bend and the double bend out-of-plane configurations details.

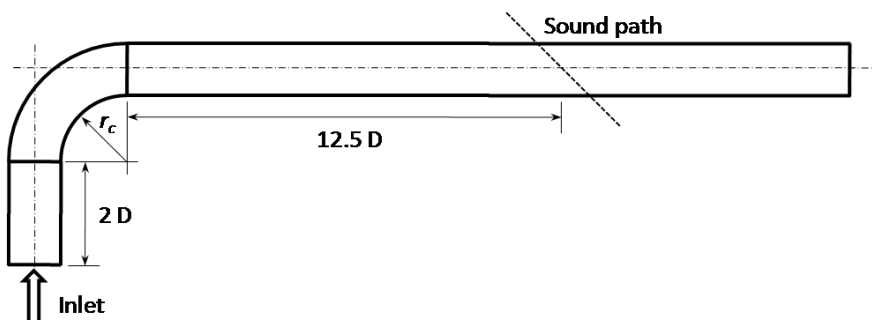


Figure 2. Single bend pipe configuration.

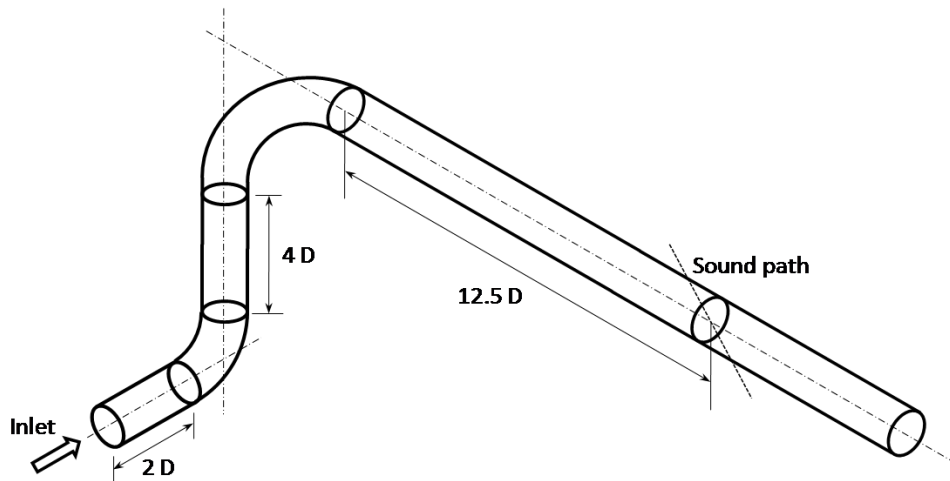


Figure 3. Double bend out-of-plane pipe configuration.

Four different curvature radii have been used for each configuration and for each case Reynolds numbers from 8,000 to 200,000 have been considered, as resumed in Tab. 2.

Table 2. Synthesis of simulated configurations.

Configuration	Curvature radius (r_c)				Reynolds number (Re)					
	0.5D	1.0D	1.5D	2.0D	8×10^3	1×10^4	2×10^4	4×10^4	1×10^5	2×10^5
Single bend										
Double bend										

A hybrid mesh has been used for numerical solutions. The mesh is unstructured in the center of the pipe where hexahedral and tetrahedral volumes are used. Over the pipe wall the mesh is structured, i.e., basically composed by prismatic volumes, in order to better representation of wall effects, as shown in Fig. 4. For each case, a mesh test has been done aiming better computational costs.

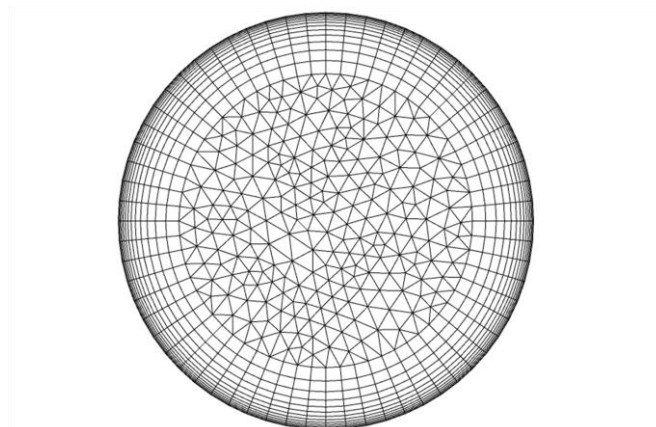


Figure 4: Hybrid mesh used for numerical solution.

2.4. Boundary conditions and fluid model

Boundary conditions are also necessary in solution of governing equations system. Here, smooth wall and no slip condition have been considered for pipe wall. Inlet condition has been set as normal uniform velocity profile so that desired Reynolds numbers were achieved. This is not the same inlet condition set by Holm *et al.* (1995), whom considered fully developed velocity and pressure field at entrance. Medium turbulence intensity at entrance domain has been supposed. Average static pressure (in the same value of reference pressure, i.e., 1 atm) has been set as overall outlet condition. Air at 25 °C has been considered in all cases. Table 3 resumes all input parameters.

Table 3. Synthesis of boundary conditions and fluid parameters.

Fluid	Air at 25 °C
Density	1.185 kg/m ³
Dynamic Viscosity	1.83 E-05 kg/m.s
Reference Pressure	1 atm
Turbulence Intensity at Entrance	Medium
Average Static Pressure at Outlet	1 atm
Wall Roughness	Smooth Wall
Wall Condition	No Slip

2.5. Numerical solution

Commercially available CFD code has been used to achieve numerical solution (ANSYS CFXTM Version 11.0, 2007). The software uses the Finite Volume Method conjugated with Multigrid technique to solve the discrete governing equations system. As convergence criteria, the root mean square (RMS) residuals of the linear solution of discretized equations are controlled to be smaller than 10⁻⁴. The advection scheme chosen was the High Resolution. All runs were performed by a PC equipped with Quad Core processor 2.4 GHz, 4.0 Gb memory and 8 Mb cache.

3. RESULTS AND DISCUSSION

Main results of all simulations are now presented and discussed. A numerical mean velocity correction factor is obtained by calculation of the mean local velocity in the direction of the sound path. CFD results allow local velocity (in nodal points) information. Since V_m and V_{SP} are known, Eq. (5) gives the numerical correction factor (k). Figures 5 shows simulated k -factor for single bend configuration for different curvature radii (0.5D-2.0D) and Reynolds numbers (8,000-200,000).

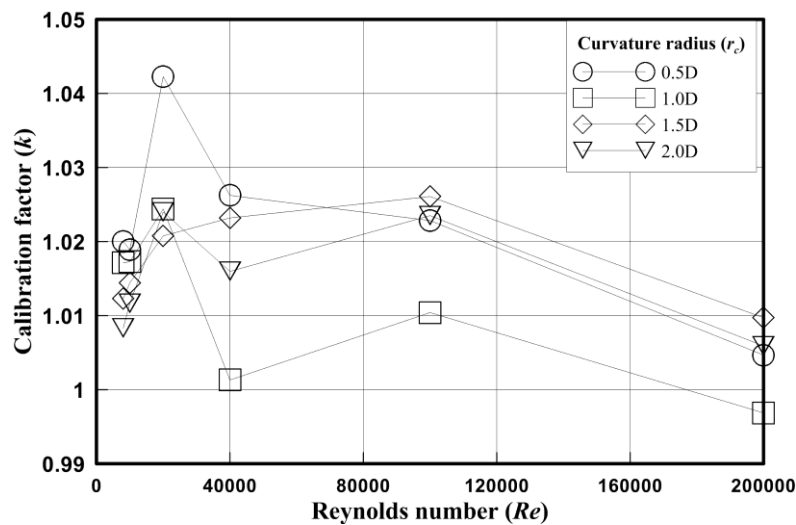


Figure 5. Simulated k -factor for Reynolds numbers from 4,000 to 200,000 and various curvature radii (single bend configuration).

For curvature radii up to 1.5D, k -factor apparently has any pattern, except for maximum values for Re 20,000. This non linear behavior may occur due to flow effects at such Reynolds number range, which is around laminar-turbulent transition. For curvature radii greater than 1.5D a decrease behavior is noticed, which indicates close proximity between the measured mean velocity and the true mean velocity.

In Fig. 6 similar results are presented, but from another point of view. Correction factor has been plotted upon an axis which represents curvature radius in diameter.

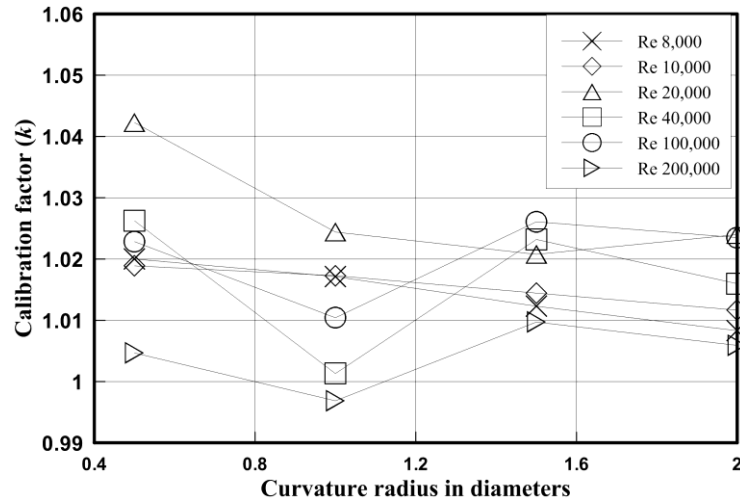


Figure 6. Simulated k-factor for varying bend curvature radius for various Reynolds numbers (single bend configuration).

Figure 6 shows that k-factors for lower Reynolds numbers (8,000-20,000) decrease for increasing curvature radii. When turbulent flow is achieved, the behavior is modified and no explicit logic pattern is observed.

For double bend configuration, simulated k-factors are greater than for those in single bend configuration. It points less propitious condition to accurate flow, probably due to swirl flow. Results for double bend configuration shows some discrepancies in Reynolds transition range when compared to single bend results. In Fig. (7) k-factors show any pattern for lower Reynolds numbers and a decreasing behavior when higher Reynolds numbers are imposed. Once again for Re=20,000, a singular behavior is observed, in this case, values smaller than the mean for each curvature radius.

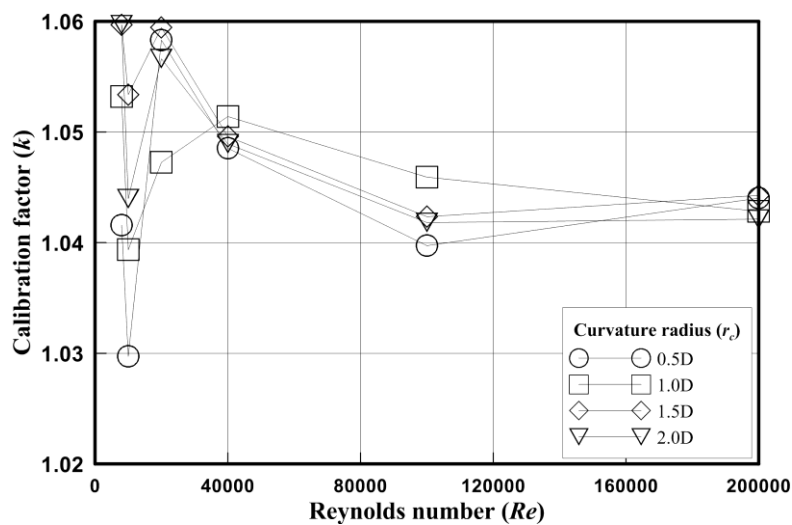


Figure 7. Simulated k-factor for Reynolds numbers from 4,000 to 200,000 and various curvature radii (double bend configuration).

As shown in Fig. 8, k-factor does not seem to present any pattern when curvature radius is changed. For lower Reynolds numbers (8,000 and 20,000) the k-factor presented the opposite tendency of Fig. (6). In single bend cases, the numerical k-factor has a decreasing behavior for this values and for the double bend configuration it increases.

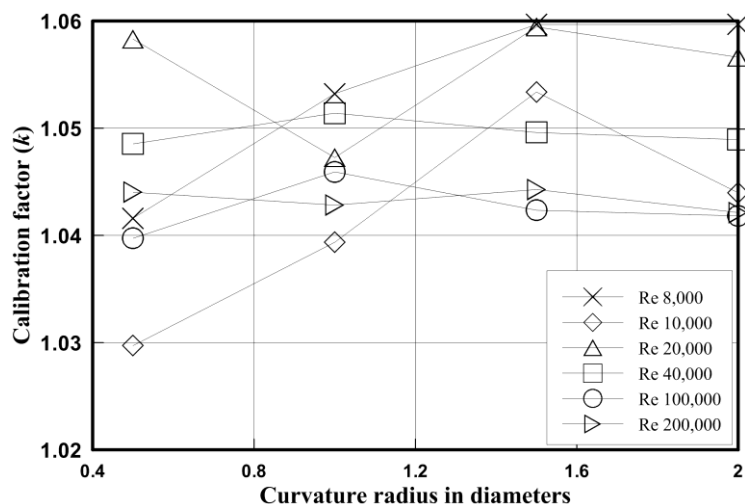


Figure 8. Simulated k-factor for varying bend curvature radius for various Reynolds numbers (double bend configuration).

4. FINAL REMARKS

Numerical simulations using CFD techniques have presented downstream flow of single bend and double bend pipe configuration. Ultrasonic numerical k-factors have been calculated for various curvature radii of such bends in order to evaluate their behavior. Any clear influence has been observed for the curvature radii and Reynolds numbers tested. These are preliminary results and other tests are still in progress. Larger Reynolds number range and other curvature radii will be simulated and discussed in the future. The use of larger diameters may also allow higher Reynolds numbers. Laminar flow is also going to be simulated aiming observation of any behavior due to curvature radius changes.

5. ACKNOWLEDGEMENTS

The authors would like to express their acknowledgments to Agência Nacional de Petróleo, Gás Natural e Biocombustíveis (ANP) for financing this project and for the grant, as well as to Laboratório de Fenômenos de Transporte Computacional (LFTC/Ufes) for the use of its computational facilities.

6. REFERENCES

- AGA Report N° 9, 1998, "Measurement of Gas by Multipath Ultrasonic Meters", American Gas Association, Washington, DC, USA.
- ANSYS CFX™ Version 11.0, 2007, ANSYS Europe Ltd.
- Hilgenstock A. and Ernst, R., 1996, "Analysis of installation effects by means of computational fluid dynamics – CFD vs experiments?", Flow Measurement Instrumentation, Vol. 7, pp. 161-171.
- Holm, M., Stang, J. and Delsing, J., 1995, "Simulation of flow meter calibration factors for various installation effects", Measurement, Vol. 15, pp. 235-244.
- Mickan, B., Wendt, G., Kramer, R. and Dopheide, D., 1997, "Systematic investigation of flow profiles in pipes and their effects on gas meter behaviour", Measurement, Vol. 22, pp. 1-14.
- Portaria Conjunta ANP/INMETRO N° 1, 2000, "Dispõe sobre Medição de Petróleo e Gás Natural", Diário Oficial da União da República Federativa do Brasil, Brasília, DF, Brazil.
- Ruppel, C. and Peters, F., 2004, "Effects of Upstream Installations on the Reading of an Ultrasonic Flowmeter", Flow Measurement and Instrumentation, Vol. 15, pp. 167-177.

7. RESPONSIBILITY NOTICE

The authors are the only responsible for the printed material included in this paper.